NANO · MICRO small
www.small-journal.com

Controlled Growth of Single-Walled Carbon Nanotube Films by Iron-assisted Floating Solid Catalyst Chemical Vapor Deposition

Xiaodan Li, Tianze Tong, Liya Zhang, Yue Yu, Mingzhi Zou, Ding Yi, Liu Qian,* Xin Gao,* and Jin Zhang**

Single-walled carbon nanotube (SWNT) films, with exciting electronic properties are increasingly important for next-generation technologies. Here, an Iron-assisted floating solid catalyst chemical vapor deposition (IA-FSCCVD) method is developed for the controlled growth of high-quality and high-purity SWNT films. Titanium carbide nanoparticles with a high melting point are used as the solid catalysts, which provide a stable template for SWNT growth through the perpendicular growth mode. Trace amounts of iron are introduced to increase the efficiency of SWNT growth. Gas chromatography measurements and density functional theory show that the gas-phase iron acts as a pre-cracking assistance for the carbon source, promoting the growth of SWNTs. Carbon nanotube films with a high quality (average I_G/I_D = 166) are successfully prepared, a small diameter deviation (mean diameter of 1.6 nm), and a high content of SWNTs (97%) using the IA-FSCCVD platform. This work provides a powerful way to prepare the carbon nanotube aggregates with a controlled structure.

1. Introduction

Decades have witnessed the rapid development of single-walled carbon nanotubes (SWNTs), which have been put on a very high pedestal in nanotechnology.[1–4] The extraordinary electrical, mechanical, and thermal properties of SWNT make it an ideal candidate for various cutting-edge fields such as transparent conductive films,[5–7] high-strength fibers,[8–10] integrated circuits,[11,12] and functional composites.[13,14] However, these exceptional properties only appear on the individual SWNT with perfect structure and high quality. Most carbon nanotube (CNT) products used today are CNT macro-structures like thin films, which contain CNTs with different wall-numbers and geometric structures, showing much lower performance than individual SWNT. As a matter of fact, it is a big challenge to transfer the outstanding properties of SWNTs from nanoscale tubes to their macroscale aggregates.[15] Therefore, realizing controlled preparation of SWNT aggregates, typically SWNT films, is of great importance.

Several methods have been developed for synthesis of free-standing CNT films, which mainly include wet and dry methods. For the wet-preparation method, the dispersed CNT solution is filtrated on a desired membrane (filtrated CNT film).[16] The structural homogeneity of this method largely depends on the CNT raw materials. The use of non-conductive surfactants, such as sodium dodecyl benzene sulfonate (SDBS), sodium dodecyl sulfonate (SDS), during the CNT dispersion leads to a complex post-processing and films with impurities, which significantly decreases their application performances. As for dry-preparation methods[15] such as super-aligned CNT arrays by domino-pushing, shear pressing, and dry drawing, the productivity is usually low. By contrast, floating catalyst chemical vapor deposition (FCCVD) method, which directly realizes the assembly and collection of CNT films at the end of the reactor,[7,10,17] is a promising approach for structure-controlled growth of CNT films because it offers more parameters to achieve better control of the catalysts and growth conditions, which is also readily to be scaled up.[18]

X. Li, T. Tong, Y. Yu, M. Zou, J. Zhang
Center for Nanochemistry
Beijing Science and Engineering Center for Nanocarbons
Beijing National Laboratory for Molecular Sciences
College of Chemistry and Molecular Engineering
Peking University
Beijing 100871, P. R. China
E-mail: jinzhang@pku.edu.cn

X. Li
Academy for Advanced Interdisciplinary Studies
Peking University
Beijing 100871, P. R. China

X. Li, L. Qian, X. Gao, J. Zhang
School of Materials Science and Engineering
Peking University
Beijing 100871, P. R. China
E-mail: qianliu-cnc@pku.edu.cn; gaoxin-cnc@pku.edu.cn

L. Zhang, D. Yi
Department of Physics
School of Physical Science and Engineering
Beijing Jiaotong University
Beijing 100044, P. R. China
E-mail: yiding@bjtu.edu.cn

The ORCID identification number(s) for the author(s) of this article can be found under https://doi.org/10.1002/smll.202402839

DOI: 10.1002/smll.202402839

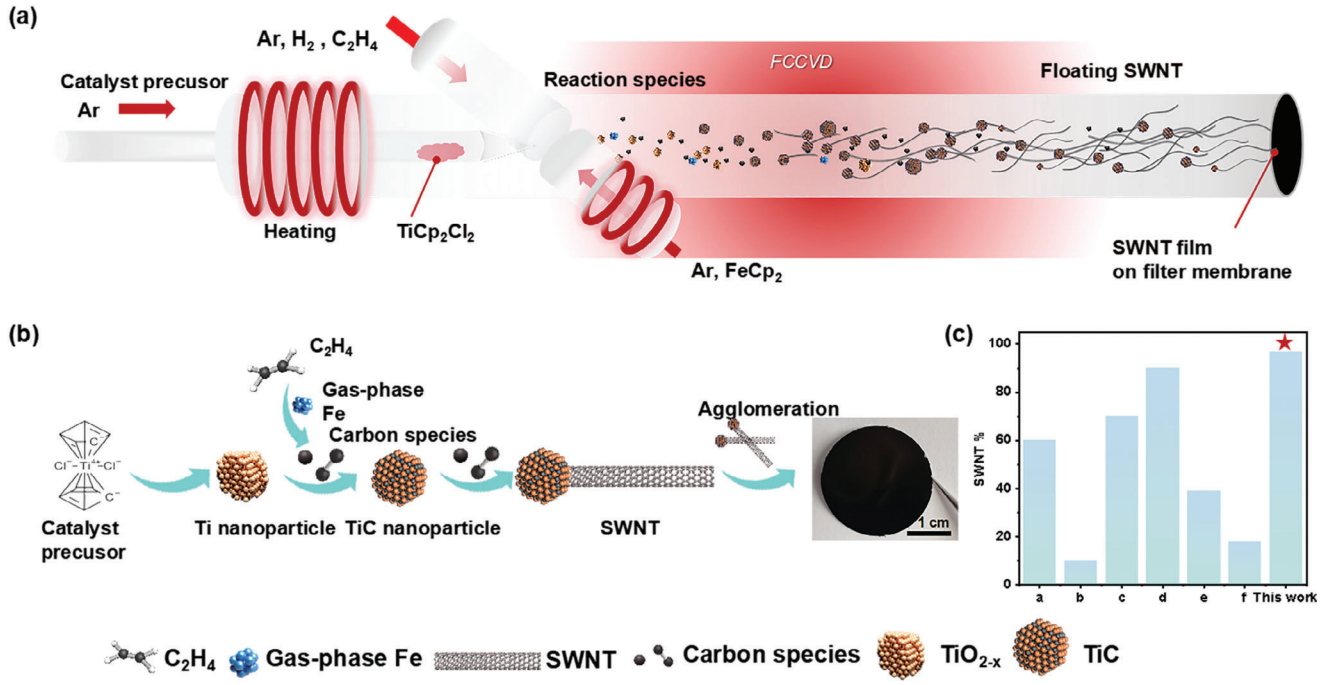

Figure 1. SWNT film preparation process. a) Illustration of the designed IA-FSCCVD system. b) The formation process of TiC catalyst with Fe assisted and the growth of SWNT film. c) The SWNT content of as-prepared CNT films using different growth methods. The horizontal axis corresponds to the entries listed in Table S1 (Supporting Information).

In a typical FCCVD method, vaporized carbon source (e.g., methane gas, isopropanol vapor), catalyst precursors (typically ferrocene), and some promotors are carried into a tube furnace by carrier gases.[19] Control of CNT wall number in FCCVD reactors has been explored by the multivariate experiments with many input factors. Fan et al. applied the FCCVD method followed by tunning the concentration of iron particles and the volume ratio of thiophene in benzene to controlled synthesize different ratio of SWNTs and multi-walled CNTs (MWNTs). Dong et al. synthesized the uniform double-walled CNTs (DWNTs) using a water-assisted FCCVD method. By changing the content of sulfur-contained promoters can also control the number of graphitic layers present in the CNT.[20] However, only over 90% SWNT content in the CNT agglomerations can be realized so far,[21] which means that the regulation of growth parameter cannot fundamentally work for the wall-number controlled synthesis. According to the growth mechanism of CNTs, such as vapor–liquid–liquid (VLS) and vapor-solid-solid (VSS) model, the structure of catalyst nanoparticles, including size, morphology, and their evolution during the FCCVD progress plays a critical role in the structure-controlled growth of SWNTs.[22,23] Most of the FCCVD process is based on iron (Fe) containing catalyst (e.g., iron–sulfur systems), in which the CNT growth followed the VLS model, and thus the CNT wall number is hard to control by Fe particles.[24–26] Therefore, the design of solid catalysts in the FCCVD system could be an effective approach to fabricate high-purity SWNT films but remains a challenge.

Recently, titanium carbide (TiC) with high-melting-point was used in a floating solid catalyst CVD (FSCCVD) system, which obtained high-purity SWNTs with specific structures on the substrates.[27–29] However, TiC with low catalytic activity decreased the production and accumulation of carbon-free radicals on catalyst nanoparticle surfaces, greatly reducing the yield and failed to realize continuous growth of SWNTs in gas phase. In this regard, here, we developed an Iron-assisted floating solid catalyst chemical vapor deposition (IA-FSCCVD) method for the controlled growth of high-quality and high-purity SWNT films. Fe with higher catalytic activity[30] was used as the co-catalyst. A small amount of sublimation-prone ferrocene ($FeCp_2$) precursors was introduced into the gas phase as auxiliary cracking aids for carbon sources,[31] improving the carbonization of TiC catalysts and the growth efficiency of SWNT growth, thereby increasing the overall yield of SWNTs. Through IA-FSCCVD method, CNT films with high purity (97%) of SWNTs and high quality were obtained, which provides a new idea for structure-controlled preparation of CNT films and other CNT aggregates.

2. Results and Discussion

2.1. Growth of High-Quality SWNTs by IA-FSCCVD System

The IA-FSCCVD system is illustrated in **Figure 1a**. In order to better expand the controllability of the floating catalytic system, we designed a three-way gas mixture, which uses a small sleeve to load the catalyst precursor, and combines with two other branches (one introducing reaction gas and the other introducing catalytic gas) to mix into the system at the inlet of the furnace. Among the various solid carbide catalysts (such as Mo_2C, WC, and TiC),[27] TiC with the higher melting point of up to 3160 °C was selected as a solid template catalyst for controlled growth

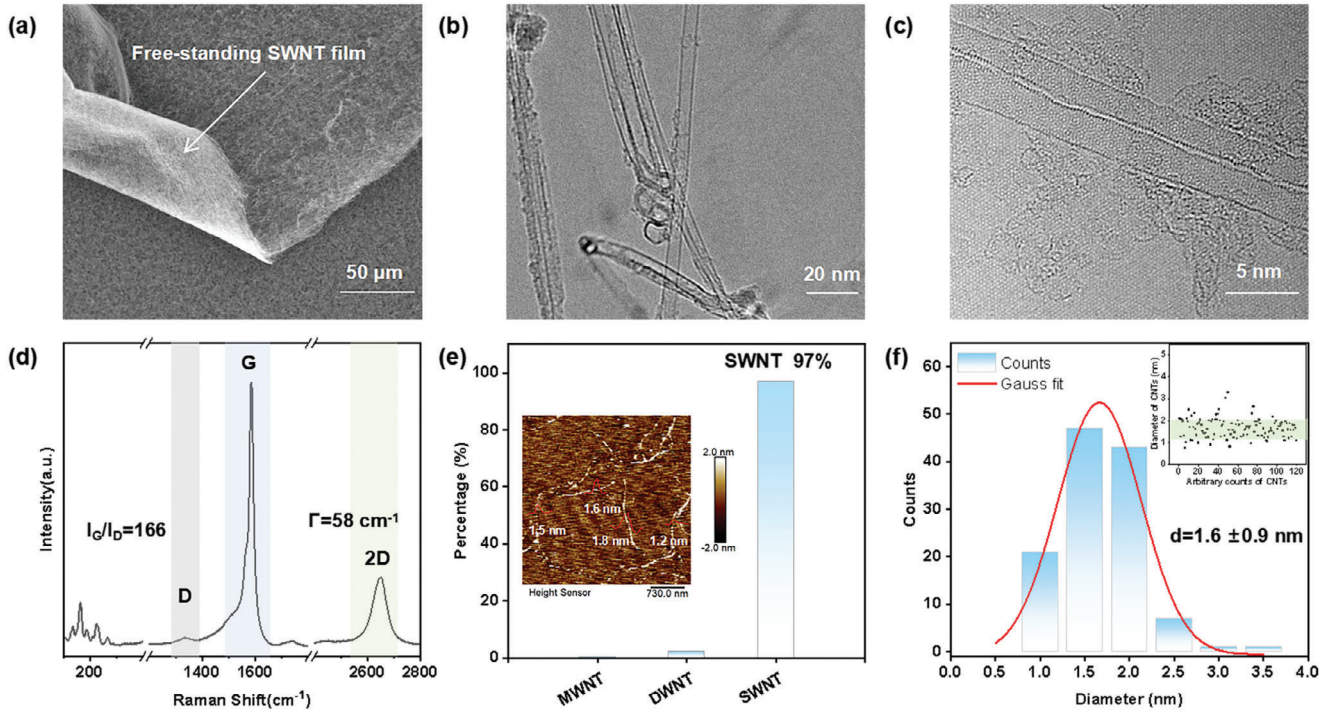

Figure 2. Characterization of as-prepared CNT film. a) SEM image of the CNT film. b,c) TEM images of the CNT in the as-growth film. d) Raman spectrum of the CNT film, was obtained using line mapping with scan step of 1um and an excitation laser of 532 nm. e) Wall number statistics of 200 CNTs. The percentage of SWNTs in the CNT film is 97%. Inset is the AFM image of the CNTs. f) The corresponding diameter distribution statistics of 200 CNTs with an average diameter of 1.6 nm. The inset shows the main diameter distribution between 1 and 2 nm.

of SWNTs. It can be directly synthesized by the Ti-containing precursor sublimating into the system carried by the hot carrier gas. The organo-metallocene compound, titanocene dichloride ($TiCp_2Cl_2$), was chosen as the Ti-based precursor. The catalyst precursor was carried into the system by hot carrier argon (Ar) gas at 250 °C (Figure S1, Supporting Information). An ultra-low Ar gas flow rate and a low heating temperature of 40 °C were used to limit the content of Fe in the gas phase to avoid the CNT nucleation and growth on Fe nanoparticles. We utilized the inductively coupled plasma-mass spectrometry (ICP-MS) to quantify the amount of Fe in the system. The results in Figure S2 (Supporting Information) show that the amount of Fe in gas phase rises linearly with the reaction time, indicating the stable supply of Fe throughout the growth process. Based on the IA-FSCCVD system, we can use different substrates at different locations in the system to obtain different forms of CNT products. For examples, the ST-cut quartz substrates used for CNT horizontal arrays in high-temperature zone, and the silicon wafer with a thin silica layer on top (SiO_2/Si) was widely used as a substrate for randomly oriented CNT networks at room temperature out of the furnace (Figure S3, Supporting Information). The as-grown CNTs in the gas phase can flow out of the reactor with the carrier gas, which makes it convenient to assemble SWNT macro-structures. A polyethersulfone filter membrane was put at the end of the quartz tube to collect CNT films. Figure 1b illustrates the decomposition of solid-state catalyst precursors, the growth and decomposition processes involving trace gas-phase Fe catalyst, resulting in the formation of a self-supporting SWNT film at the furnace exit. With the assistance of gas-phase iron in the solid catalyst CVD system, we realized the wall-number control of the CNT film with while ensuring the quality. Our method obtained a high purity of SWNTs of 97% in the film, which outperforms most previously reported works using the parameter optimization method (Figure 1c).[20,32–34]

2.2. Characterization of SWNT

We prepared free-standing SWNT networks using the IA-FSCCVD system with the TiC catalyst (**Figure 2a**). The as-prepared CNT film with a thickness of 30 μm is easily peeled off with tweezers and dry-transferred to arbitrary substrates (Figure S4, Supporting Information). The wall number of CNT in the film was measured by high-resolution transmission electron microscopy (HRTEM). Figure 2b,c shows primarily single-walled CNTs with minimal amorphous carbon on the wall. The quality and the wall-number of CNTs were further confirmed by the Raman scattering analysis (Figure 2d). The Raman spectra of as-prepared films, averaging 41 measurements at different locations, show a sharp G-band peak and a high-intensity ratio of G-band peak to D-band peak. The 2D peak presents a symmetrical peak shape with a half-peak breadth (Γ) of 58 cm^{-1}, further verifying the enrichment of single-walled CNTs.[35,36] Besides, Raman spectra of SWNTs grown with varying amounts of $FeCp_2$ (Figure S5, Supporting Information) show the effect of Fe promoter on the quality of the CNT film. Higher I_G/I_D was obtained with 100 sccm Fe (Figure S6, Supporting Information).

Wall-number statistics of 200 CNTs (Figure 2e and the corresponding TEM images shown in Supporting Information)

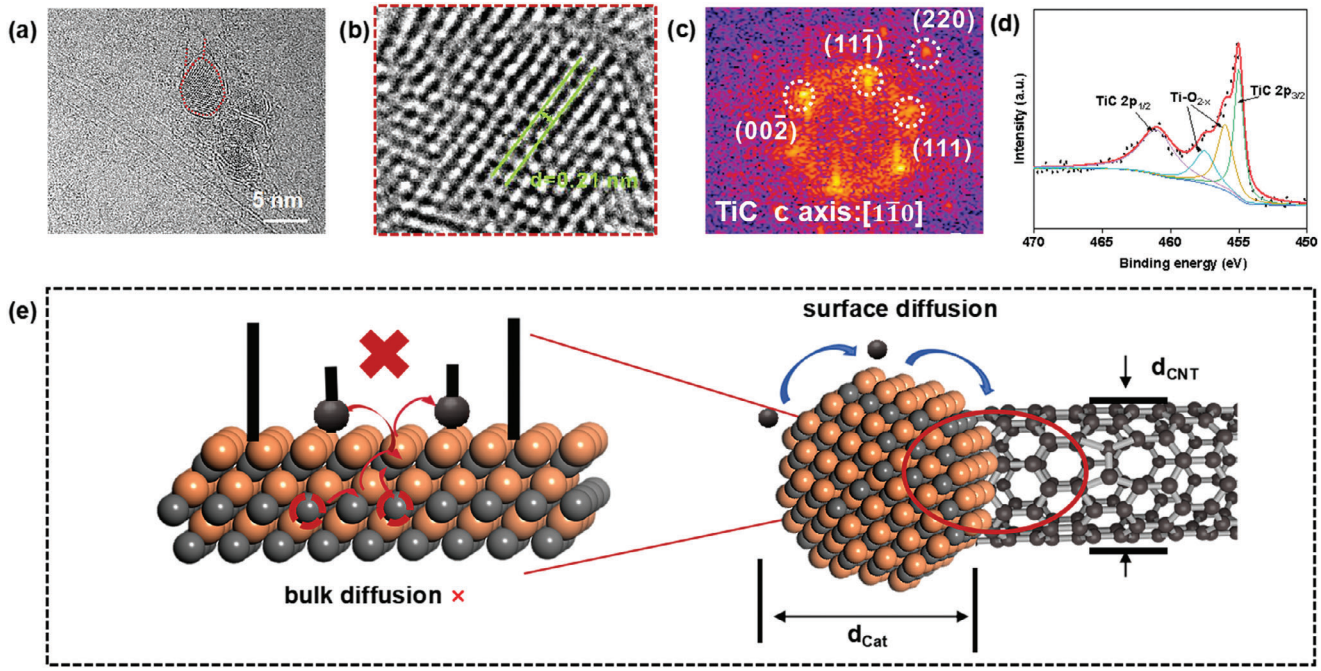

Figure 3. The mechanism of SWNT film growth. a) ACTEM image of the SWNT connected to TiC catalyst nanoparticle (traced by the red dot lines). b) Enlarged HRTEM image of the catalyst nanoparticle and (c) its corresponding FFT pattern. d) The XPS Ti 2p spectra of the SWNT film (collected on the SiO_2/Si substrate) at the end position of the furnace under the optimal growth condition. e) SWNT growth through the perpendicular growth mode.

based on TEM images show that the proportion of SWNTs, DWNTs, and triple-walled CNTs in the product was 97%, 2%, and 1%, respectively, with diameters mainly ranging from 1 to 2 nm and a peak frequency at 1.6 nm (Figure 2f). The diameter distribution of the SWNTs was further confirmed by the resonant peaks of the radial breathing mode (RBM) by the correlation of 'd (nm) = 248/v (cm^{-1})' (d: diameter, v: Raman shift).[37] Atomic force microscopy (AFM) on SiO_2/Si substrates (Figure 2e inset and Figure S7, Supporting Information) aligns with Raman and HRTEM diameter distribution results. Moreover, semi-/metallic selectivity of CNTs was further analyzed through RBM distribution (see Figure S7, Supporting Information). The percentage of semiconducting CNTs is ≈80%.

2.3. Mechanism for Controlled Growth of CNT Film

To understand the growth mechanism of CNT films using the TiC catalyst, we used spherical aberration corrected transmission electron microscopy (ACTEM) to characterize the interface between the catalyst and as-grown CNT. As shown in **Figures 3a** and S8 (Supporting Information), the SWNT perpendicularly grew along the catalyst. The ratio of the diameter of the SWNT and the catalyst nanoparticle is 0.36, aligned with the theory of the VSS mechanism and the perpendicular mode.[38] A HRTEM image of the catalyst nanoparticle is shown in Figure 3b (red frame). According to the fast Fourier transform (FFT) pattern (see Figure 3c), both the interplanar spacing and dihedral angles of the nanocrystal match well with the face-centered cubic structure of TiC. The growth direction of CNTs is perpendicular to the c axis, and we analyzed that the growth c axis is [11__0], and the catalyst model crystal plane for subsequent theoretical calculations is also selected based on this. X-ray photoelectron spectroscopy (XPS) measurements were further performed to further confirm the TiC formation. As shown in Figure 3d, Ti—C bonds (peaks at ≈455 eV for Ti $2p_{3/2}$ and at ≈461 eV for Ti $2p_{1/2}$) in the Ti 2p spectrum indicated the formation of TiC under a high temperature of 1050 °C.[39] The peak at 455.6 eV in the Ti 2p spectra, which might be attributed to Ti—O_{2-x} bonds, could be related to titanium re-oxidation in air of nanoparticles on the surface before the XPS measurement.[40] Further, we performed XPS analysis of samples at different locations in the reactor using a special protective chamber to transfer CNT samples (for details see, Figure S9, Supporting Information). The XPS results show that the introduction of trace Fe in the gas phase promotes the formation of TiC catalysts, and thus improves the yield of SWNTs in the gas phase.

Further, we analyzed the reasons why the system can control the growth of SWNTs from the perspective of thermodynamics and kinetics. In a solid carbide phase, vacancy diffusion should be the main route of carbon diffusion.[39] Due to the high melting point of 3160 °C, the bulk phase atoms of TiC nanoparticle are tightly arranged and firm at the growth temperature (1050 °C), and the carbon atoms cannot migrate from the bulk phase to achieve multi-wall growth. Consequently, the carbon flux through bulk TiC is severely restricted due to the substantial energy required for vacancy migration. The predominant mechanism for the SWNT growth is the fast carbon atoms diffusion on the surface of the TiC nanoparticles (Figure 3e), which realizes the growth of carbon nanotubes with high content of single-wall number. Our results indicate that the SWNT growth on TiC solid

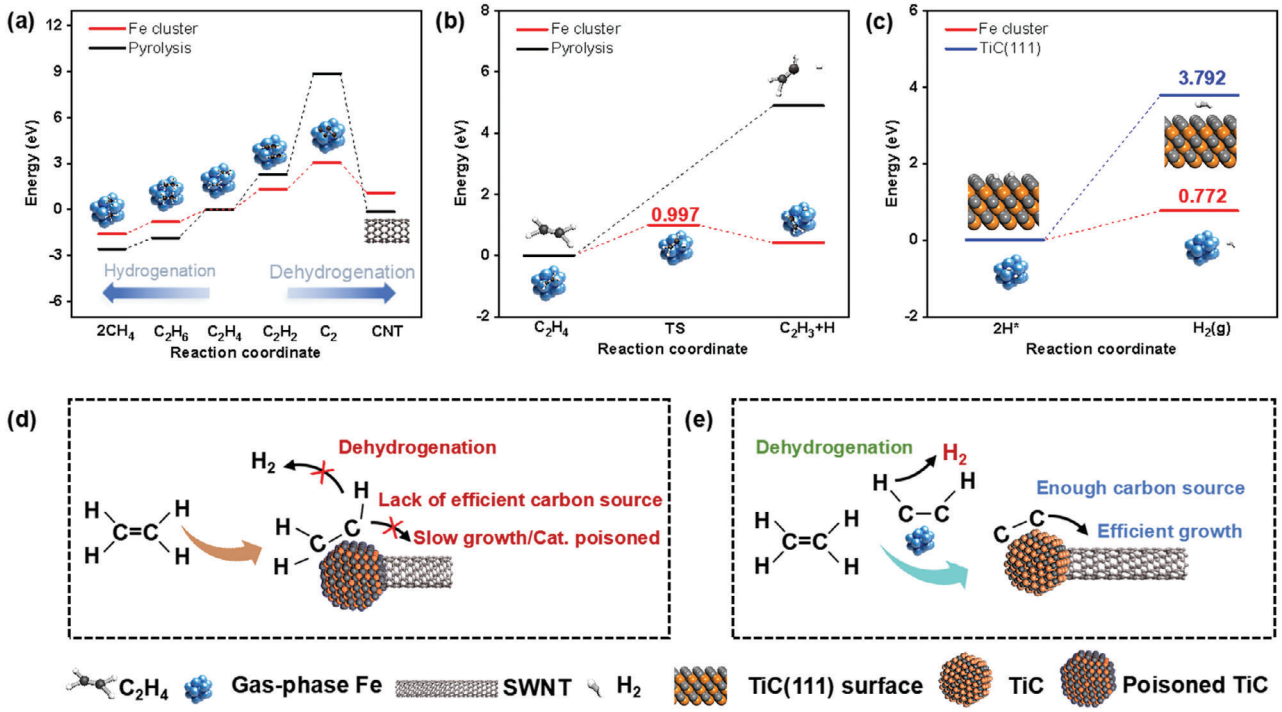

Figure 4. Theoretical calculations for efficient growth of SWNTs using IA-FSCCVD. a) Calculated energy diagram for ethylene hydrogenation (to the left) and dehydrogenation (to the right) with and without Fe cluster. b) Calculated dehydrogenation barriers with and without Fe cluster. c) Energy changes during the desorption process of H atoms from Fe and TiC surfaces. d,e) Schematic illustrations of the reaction process from ethylene dehydrogenation to SWNT growth with and without Fe-assistance.

catalysts is primarily driven by surface diffusion of carbon, following the VSS growth mechanism.

2.4. The Effect of Gas-Phase Fe for SWNT Film Growth

The aforementioned results suggest that the gas-phase Fe plays an important role in the process of carbon-source decomposition. Due to the high catalytic activity of Fe, it can be inferred that iron nanoclusters in the gas phase facilitate more thorough decomposition of the carbon source. The decomposed carbon species are primarily utilized for the growth of SWNTs, mitigating the formation of amorphous carbon, which can poison the catalyst nanoparticles, resulting in reduced efficiency in the growth of SWNTs. Therefore, gas-phase Fe effectively acts as a pre-cracking assistance for the carbon source, promoting the growth of SWNTs on other catalysts.

We vary the amount of gas-phase Fe to study its effect on the CNT growth in IA-FSCCVD system (Figures S5 and S10, Supporting Information). When the content of gas-phase Fe is insufficient to dominate CNT growth, increasing Fe content significantly enhances the CNT yield. However, excessive Fe will lead to excessive carbon source cracking, which deactivates the catalyst and subsequently reduces the CNT yield. As analyzed from the RBM peak in Raman spectra, excessive Fe in the system induces the emergence of the defect peak (D peak). Based on this, we used moderate vapor-phase Fe amount for high-quality SWNT film growth.

To gain further insights into the mechanism of this pre-cracking strategy, we conducted density functional theory (DFT) calculations for the ethylene decomposition process to elucidate the possibilities of the reactions. Based on the gas chromatography results in Figure S11 (Supporting Information), the main products of the reaction exhaust gas are methane, acetylene, and other hydrocarbon species. **Figure 4a** depicts the calculated energy diagram for ethylene hydrogenation (left) and dehydrogenation (right) with and without Fe cluster. The presence of Fe clusters significantly reduces the absorbed energy for dehydrogenation and released energy for hydrogenation of the ethylene, resulting in the promotion of the dehydrogenation of ethylene (C_2H_4) to acetylene (C_2H_2) then to carbon source (C_2). To further explore the effect of Fe cluster on ethylene dehydrogenation, we calculated the energy barrier of ethylene and acetylene dehydrogenation as shown in Figure 4b and Figure S12 (Supporting Information). With the assistance of Fe cluster, cleavage of the C—H bonds become much easier (0.997 eV vs 4.903 eV and 0.975 eV vs 5.935 eV for ethylene and acetylene dehydrogenation, respectively). Figure 4c and Figure S13 (Supporting Information) further compare the desorption (or dehydrogenation) of H atoms on the iron cluster and on the surface of the TiC nanoparticles to form H_2. It can be clearly seen that the desorption (or dehydrogenation) of H atoms on the Fe cluster is significantly lower than that on the TiC surface, which further illustrates the conclusion that Fe clusters can solve the dehydrogenation problem of the carbon source on the TiC nanoparticles. This provides a high carbon source utilization rate for the formation of TiC catalysts and the growth of CNTs. Figure 4d,e illustrates the reaction process from ethylene dehydrogenation to CNT growth without and with Fe clusters.

Fe-assisted growth ensures an ample supply of carbon sources for efficient CNT growth, whereas hydrogenation of ethylene and C—H cleavage prevails in the absence of Fe clusters on the TiC surfaces, leading to insufficient carbon sources for CNT growth (Figure 4d). The DFT calculations strongly supports our hypothesis that the gas-phase Fe effectively assists in the dehydrogenation of the carbon sources, promoting the growth of CNTs on other catalysts.

3. Conclusion

In summary, we developed an IA-FSCCVD method for structure-controlled CNT film growth. The high-melting-point solid-state TiC catalyst was prepared via gas-phase synthesis, providing a stable template for controlling the wall number of the grown CNTs. Introduction of trace Fe catalysts in the vapor phase enhanced the carbon source dehydrogenation, promoting full carburization of titanium carbide catalysts and boosting carbon nanotube growth, thereby increasing the yield. Using the IA-FSCCVD platform, a high-quality CNT film was prepared with a purity of SWNTs up to 97%. Through a combination of quasi in situ experiments and theoretical calculations, this work comprehensively elucidated the assisting mechanisms of trace iron catalysts in the gas phase, providing new insights into the selection of suitable catalysts for the controlled synthesis of SWNTs.

Supporting Information

Supporting Information is available from the Wiley Online Library or from the author.

Acknowledgements

This work was financially supported by the Ministry of Science and Technology of China (2022YFA1203302, 2022YFA1203304, and 2018YFA0703502), the National Natural Science Foundation of China (Grant Nos. 52021006, 52102032, and 52302034), the Strategic Priority Research Program of CAS (XDB36030100), the Beijing National Laboratory for Molecular Sciences (BNLMS-CXTD-202001) and the Shenzhen Science and Technology Innovation Commission (KQTD20221101115627004).

Conflict of Interest

The authors declare no conflict of interest.

Author Contributions

X.L., T.T., and L.Z. contributed equally to this work. X.L. developed the IA-FSCCVD method and prepared the SWNTs. X.L. and T.T. performed the SEM/Raman/AFM measurements. Y.Y. performed the TEM characterization. L.Z. and D.Y. performed theoretical calculations. L.Q., X.G., D.Y., and J.Z. supervised over all the experiments and data collection. All authors contributed to the discussion of data and writing of the manuscript.

Data Availability Statement

The data that support the findings of this study are available from the corresponding author upon reasonable request.

Keywords

carbon nanotube films, floating catalyst chemical vapor deposition, single-walled carbon nanotubes, solid catalysts

Received: April 9, 2024
Revised: June 24, 2024
Published online:

[1] S. Iijima, *Nature* **1991**, *354*, 56.
[2] D. S. Bethune, C. H. Kiang, M. S. de Vries, G. Gorman, R. Savoy, J. Vazquez, R. Beyers, *Nature* **1993**, *363*, 605.
[3] S. Iijima, T. Ichihashi, *Nature* **1993**, *363*, 603.
[4] M. S. Dresselhaus, *Nat. Mater.* **2004**, *3*, 665.
[5] E. X. Ding, A. Hussain, S. Ahmad, Q. Zhang, Y. Liao, H. Jiang, E. I. Kauppinen, *Nano Res.* **2019**, *13*, 112.
[6] W. B. Liu, S. Pei, J. Du, B. Liu, L. Gao, Y. Su, C. Liu, H. M. Cheng, *Adv. Funct. Mater.* **2011**, *21*, 2330.
[7] W. Ma, L. Song, R. Yang, T. Zhang, Y. Zhao, L. Sun, Y. Ren, D. Liu, L. Liu, J. Shen, Z. Zhang, Y. Xiang, W. Zhou, S. Xie, *Nano Lett.* **2007**, *7*, 2307.
[8] M. Motta, Y. L. Li, I. A. Kinloch, A. H. Windle, *Nano Lett.* **2005**, *5*, 1529.
[9] R. M. Sundaram, K. K. Koziol, A. Windle, *Adv. Mater.* **2011**, *23*, 5064.
[10] Y. L. Li, I. A. Kinloch, A. H. Windle, *Science* **2004**, *304*, 276.
[11] S. J. Tans, M. H. Devoret, H. Dai, A. Thess, R. E. Smalley, L. J. Geerligs, C. Dekker, *Nature* **1997**, *386*, 474.
[12] L. Qian, Q. Shao, Y. Yu, W. Liu, S. Wang, E. Gao, J. Zhang, *Adv. Funct. Mater.* **2022**, *32*, 2106643.
[13] Y. C. Chen, N. R. Raravikar, L. S. Schadler, P. M. Ajayan, Y. P. Zhao, T. M. Lu, G. C. Wang, X. C. Zhang, *Appl. Phys. Lett.* **2002**, *81*, 975.
[14] M. Q. Zhao, Q. Zhang, X. L. Jia, J. Q. Huang, Y. H. Zhang, F. Wei, *Adv. Funct. Mater.* **2010**, *20*, 677.
[15] W. Xu, Y. Chen, H. Zhan, J. N. Wang, *Nano Lett.* **2016**, *16*, 946.
[16] H. Zhan, Y. W. Chen, Q. Q. Shi, Y. Zhang, R. W. Mo, J. N. Wang, *Carbon* **2022**, *186*, 205.
[17] A. G. Nasibulin, A. Kaskela, K. Mustonen, A. S. Anisimov, V. Ruiz, S. Kivistö, S. Rackauskas, M. Y. Timmermans, M. Pudas, B. Aitchison, M. Kauppinen, D. P. Brown, O. G. Okhotnikov, E. I. Kauppinen, *ACS Nano* **2011**, *5*, 3214.
[18] M. Li, X. Liu, X. Zhao, F. Yang, X. Wang, Y. Li, *Top. Curr. Chem.* **2017**, *375*, 29.
[19] J. S. Bulmer, A. W. N. Sloan, M. Glerum, J. Carpena-Núñez, R. Waelder, J. Humes, A. M. Boies, M. Pasquali, R. Rao, B. Maruyama, *Carbon* **2023**, *201*, 719.
[20] S. H. Lee, J. Park, H. R. Kim, J. Lee, K. H. Lee, *RSC Adv.* **2015**, *5*, 41894.
[21] Q. Liu, W. Ren, Z. G. Chen, D.-W. Wang, B. Liu, B. Yu, F. Li, H. Cong, H.-M. Cheng, *ACS Nano* **2008**, *2*, 1722.
[22] Y. Chen, M. Lyu, Z. Zhang, F. Yang, Y. Li, *ACS Cent. Sci.* **2022**, *8*, 1490.
[23] X. Zhao, S. Sun, F. Yang, Y. Li, *Acc. Chem. Res.* **2022**, *55*, 3334.
[24] Y. Taki, K. Shinohara, M. Kikuchi, A. Tanaka, *Jpn. J. Appl. Phys.* **2008**, *47*.
[25] S. Inoue, S. Lojindarat, T. Kawamoto, Y. Matsumura, T. Charinpanitkul, *Chem. Phys. Lett.* **2018**, *699*, 88.
[26] W. H. Chiang, D. N. Futaba, M. Yumura, K. Hata, *Carbon* **2011**, *49*, 4368.
[27] S. Zhang, L. Kang, X. Wang, L. Tong, L. Yang, Z. Wang, K. Qi, S. Deng, Q. Li, X. Bai, F. Ding, J. Zhang, *Nature* **2017**, *543*, 234.
[28] S. Zhang, L. Tong, Y. Hu, L. Kang, J. Zhang, *J. Am. Chem. Soc.* **2015**, *137*, 8904.

[29] L. Qian, Y. Xie, Y. Yu, S. Wang, S. Zhang, J. Zhang, *Angew. Chem., Int. Ed.* **2020**, *59*, 10884.
[30] S. Ahmad, Y. Liao, A. Hussain, Q. Zhang, E. X. Ding, H. Jiang, E. I. Kauppinen, *Carbon* **2019**, *149*, 318.
[31] T. Tong, W. Liu, J. Yan, M. Zou, L. Qian, J. Zhang, *Carbon* **2023**, *205*, 27.
[32] Y. Y. Fan, A. Kaufmann, A. Mukasyan, A. Varma, *Carbon* **2006**, *44*, 2160.
[33] J. Wei, H. Zhu, Y. Jia, Q. Shu, C. Li, K. Wang, B. Wei, Y. Zhu, Z. Wang, J. Luo, W. Liu, D. Wu, *Carbon* **2007**, *45*, 2152.
[34] Q. Jiang, F. Wang, R. Li, B. Li, N. Wei, N. Gao, H. Xu, S. Zhao, Y. Huang, B. Wang, W. Zhang, X. Wu, S. Zhang, Y. Zhao, E. Shi, R. Zhang, *Nano Lett.* **2023**, *23*, 523.
[35] A. Jorio, C. Fantini, M. S. S. Dantas, M. A. Pimenta, A. G. Souza Filho, G. G. Samsonidze, V. W. Brar, G. Dresselhaus, M. S. Dresselhaus, A. K. Swan, et al., *Phys. Rev. B* **2002**, *66*.
[36] P. Puech, E. Flahaut, A. Bassil, T. Juffmann, F. Beuneu, W. S. Bacsa, *J. Raman Spectrosc.* **2007**, *38*, 714.
[37] A. Jorio, R. Saito, J. H. Hafner, C. M. Lieber, M. Hunter, T. McClure, G. Dresselhaus, M. S. Dresselhaus, *Phys. Rev. Lett.* **2001**, *86*, 1118.
[38] M. F. C. Fiawoo, A. M. Bonnot, H. Amara, C. Bichara, J. Thibault-Peenisson, A. Loiseau, *Phys. Rev. Lett.* **2012**, *37*, 195503.
[39] L. Zhang, R. V. Koka, *Mater. Chem. Phys.* **1998**, *57*, 23.
[40] A. A. El Mel, B. Angleraud, E. Gautron, A. Granier, P. Y. Tessier, *Thin Solid Films* **2011**, *519*, 3982.